Probing quantum and thermal noise in an interacting many-body system

S. HOFFERBERTH[1,2,3], I. LESANOVSKY[2,4], T. SCHUMM[1], A. IMAMBEKOV[3,5], V. GRITSEV[3], E. DEMLER[3] AND J. SCHMIEDMAYER[1,2]*

[1]Atominstitut der Österreichischen Universitäten, TU-Wien, Stadionallee 2, A-1020 Vienna, Austria
[2]Physikalisches Institut, Universität Heidelberg, Philosophenweg 12, D-69120 Heidelberg, Germany
[3]Department of Physics, Harvard University, Cambridge, Massachusetts 02138, USA
[4]Institut für Theoretische Physik, Universität Innsbruck, Technikerstr. 21a, A-6020 Innsbruck, Austria
[5]Department of Physics, Yale University, New Haven, Connecticut 06520, USA
*e-mail: schmiedmayer@atomchip.org

Published online: 20 April 2008; doi:10.1038/nphys941

The probabilistic character of the measurement process is one of the most puzzling and fascinating aspects of quantum mechanics. In many-body systems quantum-mechanical noise reveals non-local correlations of the underlying many-body states. Here, we provide a complete experimental analysis of the shot-to-shot variations of interference-fringe contrast for pairs of independently created one-dimensional Bose condensates. Analysing different system sizes, we observe the crossover from thermal to quantum noise, reflected in a characteristic change in the distribution functions from poissonian to Gumbel type, in excellent agreement with theoretical predictions on the basis of the Luttinger-liquid formalism. We present the first experimental observation of quasi-long-range order in one-dimensional atomic condensates, which is a hallmark of quantum fluctuations in one-dimensional systems. Furthermore, our experiments constitute the first analysis of the full distribution of quantum noise in an interacting many-body system.

The probabilistic nature of Schrödinger wavefunctions and the uncertainty principle are crucial aspects of the modern understanding of quantum matter. Starting with the famous Bohr–Einstein debates, intrinsic quantum-mechanical noise has been the subject of numerous discussions and controversies[1] and the starting point of many new developments: the analysis of noise in non-classical states of light was an important step towards the foundation of quantum optics[2]. In solid-state systems current fluctuations enable us to probe the nature of electrical transport in mesoscopic systems[3,4] and to investigate quantum correlations and entanglement in electron interferometers[5,6]. In atomic physics, noise correlation analysis[7] was used to study quantum states in optical lattices[8,9], pair correlations in Fermi gases[10], the counting statistics in an atom laser[11] and the Hanbury Brown–Twiss effect for both bosons and fermions[12,13].

Interference experiments provide a different powerful tool, which was used, for example, to study critical fluctuations[14], thermal fluctuations in elongated condensates[15] and the Berezinskii–Kosterlitz–Thouless transition in a two-dimensional quantum gas[16]. Recently, it has been suggested that the full statistics of fluctuations in the contrast of interference fringes can be used to probe high-order correlation functions and reveal non-trivial phases of low-dimensional condensates[17,18].

Here we combine the two ideas and investigate the interplay between quantum and thermal noise in one-dimensional (1D) systems. Earlier experiments with weakly interacting Bose gases have studied thermal noise by phase[15,19] and density[20] fluctuations in the 1D–3D crossover, whereas experiments with 1D condensates in optical lattices observed manifestations of strong correlations in the three-body recombination rate[21], the total energy[22] and the momentum distribution of atoms[23]. In our experiments we analyse the shot-to-shot variations in the interference of two independently created 1D condensates. For large system sizes we find that both the average contrast and its variations are dominated by thermal fluctuations. For short system sizes we demonstrate that the distribution functions of fringe contrast provide unambiguous signatures of quantum fluctuations. Our results provide a clear demonstration of quasi-long-range order and the power-law nature of the correlation functions, which is the hallmark of 1D quasi-condensates. It constitutes the first measurements of the full distribution functions of quantum noise in an interacting many-body system.

EXPERIMENTAL PROCEDURE

Our experiments are carried out using two independent 1D quantum degenerate atomic Bose gases created in a radio-frequency-induced microtrap[24–26] on an atom chip[27,28]. Each sample contains typically 3,000–5,000 atoms in the 1D regime[29,30], with both temperature $T < 80\,\mathrm{nK}$ and chemical potential $\mu \approx h \times 1\text{–}2\,\mathrm{kHz}$ fulfilling $k_B T, \mu < h\nu_\perp$, where $\nu_\perp = 3.0\,\mathrm{kHz}$ is the trapping frequency of the harmonic transverse confinement. When the two independent 1D condensates are released, they recombine in time of flight and the resulting interference pattern is recorded using standard absorption imaging (Fig. 1a).

Examples of the observed fringe patterns are shown in Fig. 1b. Although the interference patterns have high local contrast, the interference fringes as a whole are not straight lines. This meandering character shows that the relative phase between the two condensates is not constant but fluctuates from point to point.

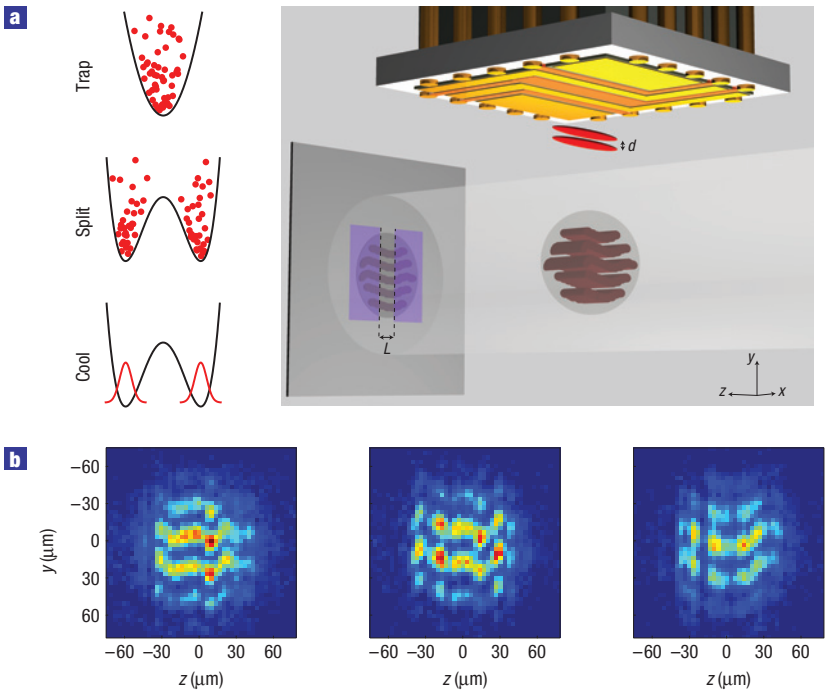

Figure 1 Experimental set-up and observed interference patterns. a, Two independent 1D Bose gases are created by first splitting a single highly elongated magnetic trap on an atom chip holding a thermal ensemble of atoms into a double well using radio-frequency-induced potentials. In a second step the separate parts are evaporatively cooled to degeneracy, producing two individual 1D condensates (schematic diagram on the left). The two systems are then simultaneously released from the trapping potential and the resulting interference pattern is recorded with standard absorption imaging. The vertical orientation of the initial system is chosen so that the interference pattern can be imaged along its transverse direction, parallel to the atom chip (illustration on the right). **b**, Colour-coded images of the resulting density patterns. The observed interference fringes show a meandering over the length of the system (*z* direction), which is due to the local differences in relative phase between the two original 1D condensates. Consequently, this waviness of the patterns contains information about the phase correlations in the individual condensates.

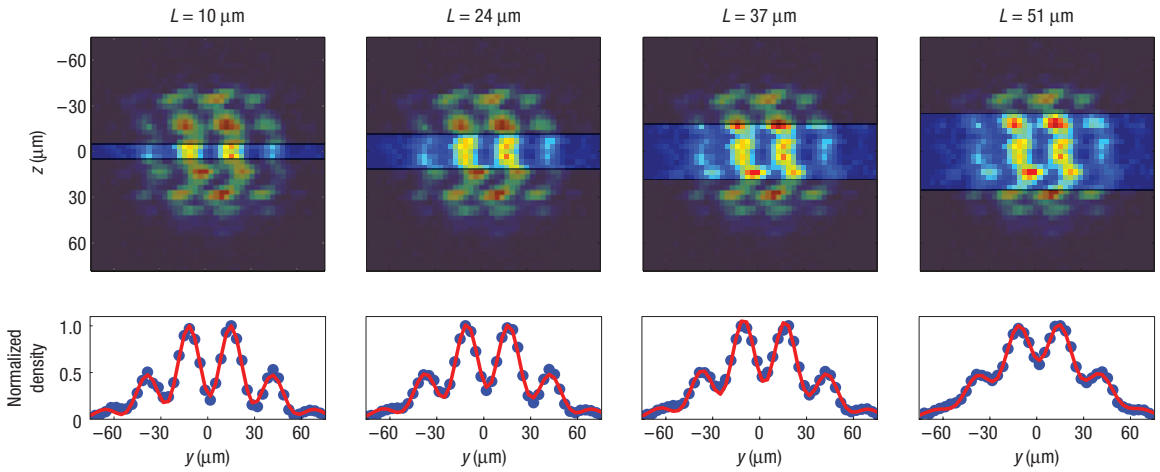

Figure 2 Analysis of the observed interference patterns. For quantitative analysis, we integrate over central slices of varying length *L* of the density profiles in the longitudinal direction as indicated by the shading in the top row, to obtain multiple transverse line-density profiles. We then extract the interference amplitude $|A_0|$ by Fourier transforming these profiles and extracting the Fourier coefficient corresponding to the fringe spacing *Q*. To illustrate contrast reduction with increasing *L*, the fringe patterns shown in the bottom row are normalized. Modulated cosine fits to these profiles then yield contrasts $C(L)$, which decrease with *L*. Note that the interference amplitude $|A_0|$ as defined in equation (1) is related to this contrast as $|A_0| = n_{1D}\, L \times C$. Consequently, as can be seen from equation (2), $|A_0(L)|$ increases with *L*, whereas the contrast $C(L)$ decreases with *L*.

These phase variations originate from both quantum and thermal fluctuations in the original 1D condensates and reflect the non-mean-field character of low-dimensional systems. Integrating local interference patterns over a finite length *L* leads to summing interference patterns that are not in phase with each other and results in a reduction of the total fringe contrast (Fig. 2). This reduction of the interference contrast, and its statistical fluctuations, contains important information about the phase

correlations of the individual 1D condensates and is the main quantity addressed in this work.

THEORETICAL MODEL

Before we proceed to the statistical analysis of the experimental data we present a quick overview of the theoretical foundations of our study. The analysis is carried out in two steps. In the first step we analyse the average amplitude of interference fringes as a function of the integration length L; the second step then analyses the quantum and thermal noise contributions to the shot-to-shot fluctuations in the average contrast.

Our interference patterns show a periodic density modulation at the interference wavevector $Q = md/\hbar t$, where m is the mass of the atoms, d is the in-trap separation of the two 1D systems and t is the expansion time. Assuming ballistic expansion, the complex amplitude of this density modulation after integration over a length L is given by[17,31]

$$A_Q(L) = \int_{-L/2}^{L/2} \mathrm{d}z\, a_1^\dagger(z) a_2(z). \qquad (1)$$

Here $a_{1,2}$ are the boson annihilation operators within the two original 1D condensates before the expansion. The phase of $A_Q(L)$ describes the position of interference fringes and is determined by the relative phase between the two condensates averaged between $-L/2$ and $+L/2$.

Because we carry out interference experiments with independent condensates, the phase of A_Q is random, and the expectation value $\langle A_Q \rangle$ is zero. This does not imply the absence of fringes but shows the unpredictable random phase in individual interference patterns[32–34]. Consequently, to study the contrast statistics of the interference patterns we have to consider the quantity $\langle |A_Q(L)|^2 \rangle$. This quantity is independent of the overall phase difference but is strongly affected by phase twisting within each condensate.

In the case of ideal non-fluctuating condensates we expect to find perfect contrast for any size of the system. This implies $\langle |A_Q(L)|^2 \rangle \propto L^2$. In the opposite regime of short-range phase correlations with finite correlation length ξ_ϕ, the net interference pattern comes from adding up fringes in L/ξ_ϕ uncorrelated domains. In this case the net interference pattern is strongly suppressed and appears only as a square root fluctuation, $\langle |A_Q(L)|^2 \rangle \propto L\xi_\phi$.

More precisely, $\langle |A_Q(L)|^2 \rangle$ is determined by the integral of the two-point correlation function:

$$\langle |A_Q(L)|^2 \rangle = \int_{-L/2}^{L/2} \mathrm{d}z_1 \int_{-L/2}^{L/2} \mathrm{d}z_2\, \langle a_1^\dagger(z_1) a_1(z_2) \rangle \langle a_2^\dagger(z_2) a_2(z_1) \rangle.$$

A special feature of 1D systems of interacting bosons is the dramatic enhancement of fluctuations. Even at $T = 0$, true long-range order is not possible and only quasi-condensates with a power-law decay of the correlation function $\langle a^\dagger(z_2) a(z_1) \rangle$ exist[35]. At finite temperatures we find exponential decay of the correlation function for distances $|z_2 - z_1|$ exceeding a thermal correlation length[29] $\xi_\phi(T)$.

To adequately describe these systems, a beyond-mean-field theory is required. A powerful non-perturbative approach that describes the long-distance behaviour of the correlation functions of 1D systems is the Luttinger liquid theory (see the Methods section and refs 36–38), on which we base our further analysis.

Using a standard expression for the two-point correlation function in Luttinger liquid theory we obtain

$$\langle |A_Q(L)|^2 \rangle = n_{1D}^2 L^2 \left(\frac{\xi_h}{L} \right)^{1/K} f\left(\frac{\xi_\phi(T)}{KL}, K \right). \qquad (2)$$

Here, $K = \pi\hbar\sqrt{n_{1D}/gm}$ is the Luttinger parameter for the weakly interacting 1D Bose gas, with n_{1D} being the 1D line density, $g = 2h\nu_\perp a_s$ the effective 1D coupling constant and a_s the s-wave scattering length. $\xi_h = \hbar/\sqrt{mgn_{1D}}$ is the healing length and $\xi_\phi(T) = \hbar^2 n_{1D}\pi/mk_B T$ is the thermal correlation length of the 1D condensates (for the weakly interacting regime). The function $f(x, K)$ is given by

$$f(x, K) = \int_0^1 \int_0^1 \mathrm{d}u\, \mathrm{d}v \left(\frac{\pi}{x \sinh(\frac{\pi|u-v|}{x})} \right)^{1/K}. \qquad (3)$$

It shows how quantum and thermal fluctuations in the 1D condensates affect $\langle |A_Q(L)|^2 \rangle$. Note that the finite number of particles can in principle lead to corrections to equation (3) (refs 31,39). We checked that for our parameters this shot noise is of no importance even for the smallest L we investigate.

Let us first discuss the case of low temperatures and/or small system sizes ($L/\xi_\phi(T) \leq 1$). Here we need to consider only quantum fluctuations, which originate from interactions between atoms. Non-interacting bosons at zero temperature have no phase fluctuations; their interference patterns show perfect contrast, leading to $\langle |A_Q(L)|^2 \rangle \propto L^2$. In the other extreme, impenetrable bosons (Tonks–Girardeau gas) have very strong fluctuations and their interference pattern corresponds to short-range correlations, $\langle |A_Q(L)|^2 \rangle \propto L$ (see the discussion above equation (2)). For finite interaction strength we find something in between, resulting in the scaling $\langle |A_Q(L)|^2 \rangle \propto L^{2-1/K}$.

Finite temperature introduces thermal fluctuations, which create phase fluctuations with a temperature-dependent correlation length $\xi_\phi(T)$. When $L > \xi_\phi(T)$, thermal fluctuations dominate and the interference amplitude scales as $\langle |A_Q(L)|^2 \rangle \propto L\xi_\phi(T)$.

The experimentally observed interference patterns provide us with more information than just the average value $\langle |A_Q(L)|^2 \rangle$. As a second step of our analysis we consider the shot-to-shot fluctuations of individual measurements, which are characterized by the higher moments $\langle |A_Q|^{2n} \rangle$ and ultimately by the entire distribution function $W(|A_Q(L)|^2)$. To visualize the shot-to-shot fluctuations of the interference amplitude, it turns out to be convenient to consider the normalized variable $\alpha(L) = |A_Q(L)|^2/\langle |A_Q(L)|^2 \rangle$ and its distribution function $W(\alpha(L))$. The importance of the higher moments $\langle |A_Q|^{2n} \rangle$ is that they are directly related to the higher-order correlation functions of the 1D interacting Bose gas[17].

In the following, we summarize only the scaling of the distribution function; a formal theoretical approach is discussed in the Methods section. In the case of non-interacting ideal condensates, that is, perfect interference patterns in each measurement, the distribution function $W(\alpha(L))$ approaches a delta function. When interactions are weak but finite, we expect a narrow distribution of width $1/K$ and $W(\alpha(L))$ to approach a universal Gumbel-like distribution[31,40]. In the limit of long integration lengths, $L \gg \xi_\phi(T)$, thermal fluctuations dominate. As discussed above, in this case the net interference pattern comes from adding local interference patterns from many uncorrelated domains, resulting in the distribution function being poissonian. For integration lengths comparable to $\xi_\phi(T)$ both quantum and thermal fluctuations are important. In this regime we expect $W(\alpha(L))$ to show a double-peak structure, with the peak at small amplitudes coming from the thermal noise and the peak at finite amplitude from quantum noise.

ANALYSIS OF THE AVERAGE INTERFERENCE AMPLITUDE

We now turn to the analysis of our experimental data, starting with the average interference amplitude square $\langle |A_Q|^2 \rangle$ and its variation with system size L.

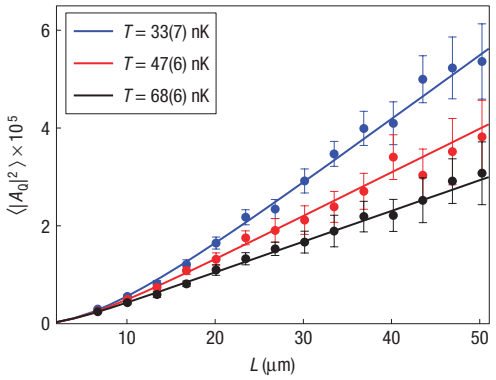

Figure 3 Length dependence of the average contrast. The data points show the measured $\langle|A_Q|^2\rangle$ for three different temperatures T. Error bars indicate the s.e.m. Each data point contains 50 individual interference measurements. The solid lines are fits of equation (2) to the data with T as free parameter (see the Methods section). K and ξ_h are determined independently from measurements of n_{1D} and $\nu_\perp$.

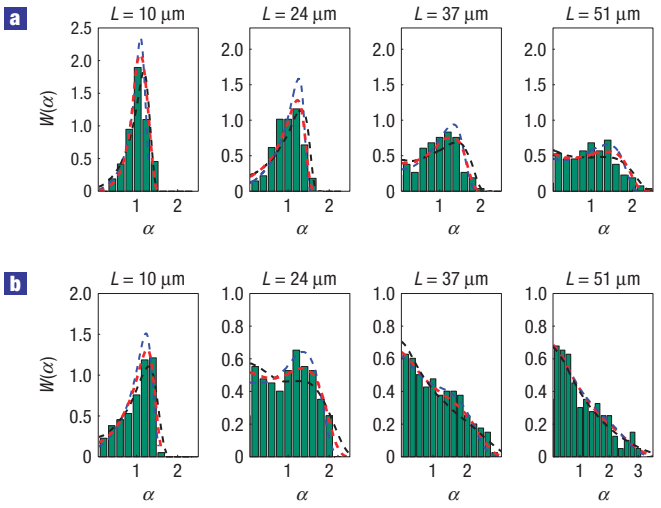

Figure 4 Distribution functions of the measured interference contrasts for different lengths L. a, The length-dependent normalized interference contrasts $\alpha(L) = |A_Q(L)|^2 / \langle|A_Q(L)|^2\rangle$ of 170 individual experimental realizations with identical parameters ($n_{1D} = 59(5)\ \mu m^{-1}$, $\nu_\perp = 3{,}020(10)$ Hz, $K = 46$) are shown as histograms. The red curves show the corresponding calculated distributions for $T = 31$ nK ($\xi_\phi(T) = 35\ \mu m$). The blue (black) curves show the calculated distributions for the upper (lower) error bounds $F \pm \Delta F$. These error estimates include uncertainties in the experimental parameters n_{1D}, $\nu_\perp$ and L and the temperature T determined from the contrast averages. The resulting error on F is $\Delta F/F \approx 15\%$. **b**, Histograms of 200 individual measurements with the same parameters as in **a**, but higher temperature $T = 60$ nK ($\xi_\phi(T) = 18\ \mu m$). For both sets we observe very good agreement between experiment and theory. In particular, the predicted change of overall shape of the distribution functions from single peak to poissonian with decreasing $F = \xi_\phi(T)/L$ (increasing L and T) is very well reproduced by the experimental data.

To extract $|A_Q|$ from the observed interference patterns, we first obtain transverse density profiles integrated over the longitudinal direction for different lengths L, as shown in Fig. 2. We then fit a cosine function with a gaussian envelope to the resulting fringe profiles to extract the relative phase and the interfering amplitude $|A_Q|$ as functions of L (see the Methods section). To ensure homogeneous 1D density, we restrict our analysis to the central 50% of the system. In this region the longitudinal confinement is well approximated by a harmonic potential with oscillator frequency $\nu_\parallel \approx 5$ Hz. For the largest L considered, $n_{1D}(z)$ varies at most by ~15% from the peak density at the trap centre. This modulation is ignored and we obtain a single value for n_{1D} by averaging over the atomic density in this centre region.

Figure 3 shows the experimentally observed average interference amplitude squares $\langle|A_Q|^2\rangle$ for three different temperatures, with the density $n_{1D} = 50(4)\ \mu m^{-1}$ and the transverse trapping frequency $\nu_\perp = 3{,}020(10)$ Hz ($\mu \approx h \times 1.5$ kHz, $K = 42$ and $\xi_h = 0.3\ \mu m$) identical for all three data sets. The higher-temperature data sets are obtained by waiting for different times after the initial preparation of the two condensates. During this waiting time, the system heats owing to residual noise in the magnetic trapping fields.

To compare measurement and theory, we fit the function equation (2) to the experimental data (Fig. 3) with the temperature T as a free parameter (see the Methods section). We find the functional behaviour of the measured contrasts to be in very good agreement with the theoretical predictions. This is of particular interest, as the shape of these curves is determined by both the quantum and thermal contributions to the average contrast, as discussed above. For integration length longer than 20–30 μm we observe a linear dependence of $\langle|A_Q(L)|^2\rangle$ on L. This corresponds to the $L \gg \xi_\phi(T)$ regime where thermal fluctuations dominate.

For shorter segment lengths, quantum fluctuations are important. However, the analysis presented in Fig. 3 is not sufficient to make the case for quantum fluctuations. The Luttinger parameter for our system is $K = 42$, and it is impossible to observe the $L^{-1/K}$ correction to the ideal-case (noise-free) power law L^2 in the limited range of lengths available. From Fig. 3 we cannot prove that fluctuations are present at all for such small system sizes. We will address this in the next part of our analysis by demonstrating that quantum fluctuations are manifest unambiguously in the shot-to-shot fluctuations of $|A_Q(L)|^2$, rather than in the $\langle|A_Q(L)|^2\rangle$ average value.

From the fits we obtain the temperatures $T = 33(7)$, $47(6)$ and $68(6)$ nK for 0, 50 and 100 ms waiting time, respectively. The increase of the temperature with longer waiting times is consistent with the heating rates in our experiments determined at higher T. We note here that this method measures the temperature of collective excitation in the condensate. We cannot confirm that this temperature is identical to that of the residual thermal atoms in the trap. Reliable detection of the thermal background is possible only down to $T \approx 80$ nK in our set-up.

The contrast method we present here can be used to measure the temperature of collective modes of 1D Bose gases at extremely low temperatures and small atom numbers, suggesting the usefulness of this method for precise thermometry of 1D condensates when conventional methods fail.

ANALYSIS OF THE FULL DISTRIBUTION FUNCTIONS

We now analyse the full information contained in the statistics of the interference contrast.

In Fig. 4, we show histograms of the measured distributions $W(\alpha(L))$ for four different length scales L and two different temperatures, $T = 31(6)$ nK (upper row, Fig. 4a) and $T = 60(5)$ nK (lower row, Fig. 4b), obtained using the contrast average method discussed in the previous section. For these data sets we determine density and transverse confinement as $n_{1D} = 59(5)\ \mu m^{-1}$ and $\nu_\perp = 3{,}020(10)$ Hz, resulting in $\mu \approx h \times 1.9$ kHz and $K = 46$.

For a detailed comparison between measurement and theory, we numerically calculate the distribution functions for the

corresponding experimental parameters for each histogram (see the Methods section and ref. 41). We emphasize that once we know the temperature of the system there are no free parameters remaining in this analysis. It is remarkable that the experimentally measured distribution functions are in such excellent agreement with the theoretical prediction (Fig. 4). In particular, we clearly observe the transition from the regime dominated by quantum fluctuations for small L at low temperature to the one dominated by thermal fluctuations for large L and higher temperature.

More quantitatively, the shape of the distribution functions is determined by a single dimensionless parameter $F = \xi_\phi(T)/L$. For large F, accessed either at low temperature T or small system length L, we find a single asymmetric peak in the distribution function $W(\alpha)$, resulting from a universal extreme-value-statistics Gumbel-like distribution[31,40], which is a smoking-gun signature of quantum fluctuations and the power-law behaviour of the correlation functions.

The Gumbel distribution has a characteristic asymmetric shape and typically appears when describing rare events such as stock market crashes or earthquakes, which go predominantly in one direction. This suggests that suppression of the contrast of interference fringes due to quantum fluctuations is dominated by rare but strong fluctuations of the phase of the bosonic fields $a_{1,2}(z)$. Most of the time we find very small phase meandering, which does not affect the contrast significantly. Only occasionally is there a strong fluctuation leading to a noticeable decrease of the interference fringe contrast.

For larger system sizes L and higher temperatures T, we observe that the distribution functions become poissonian, characteristic for the dominance of thermal fluctuations and the exponentially decaying correlations. The system can be thought of as consisting of domains of size $\xi_\phi(T)$, with uncorrelated phases in each of the domains. In this case, adding up interference amplitudes (complex numbers) is similar to carrying out a random walk in two dimensions, and the total amplitude (distance travelled) is proportional to the number of steps, resulting in the net interference contrast being proportional to $1/\sqrt{L}$.

Finally, for intermediate lengths and temperatures, we observe the formation of a double-peak structure in the distribution functions, characterized by a peak at zero, originating from thermal noise, and a peak at finite amplitude α originating from quantum noise[31,41]. In this crossover regime the relative effects of quantum fluctuations are diminished but not completely suppressed, so that both quantum and thermal fluctuations are of importance in determining the shape of the distribution functions. We also find very good agreement between experiment and theory in this crossover regime.

DISCUSSION AND SUMMARY

It is interesting to note that the above analysis is based on the Luttinger liquid theory of interacting bosons in one dimension, which is accurate for calculating the long-range part of the correlation functions but does not capture the short-distance part on the scale of the healing length ξ_h. For system size $L \gg \xi_h$ it is this long-distance part of the correlation functions that gives the dominant contribution to the integrals determining the interference amplitude (see equation (2)). This sensitivity to the long-distance part of the correlation functions is the unique feature of interference experiments, which makes them a powerful tool for analysing quantum and thermal fluctuations in low-dimensional condensates.

Alternative approaches, such as measurements of density fluctuations in expanding condensates[19], probe correlation functions on the scale of the healing length. This short-range part of the correlation function is hardly sensitive to the quasi-long-range nature of quantum fluctuations in 1D systems. This makes it difficult to observe quantum effects by direct measurement of density fluctuations: they reveal the role of interactions[20] but the transformation of short-range correlations into density fluctuations masks the quantum correlations.

In summary, we have studied quantum and thermal noise in 1D systems of interacting quantum degenerate bosons using the full distribution function of the interference amplitude. The shot-to-shot fluctuations in the contrast contain information that can be related to high-order correlation functions of the 1D system. Our results provide the first experimental measurements of the full distribution function of quantum noise in an interacting many-body system. By analysing these distribution functions we provide direct experimental evidence of quasi-long-range order in 1D condensates. The remarkable agreement between our experimental findings and theoretical predictions on the basis of Luttinger liquid model provides an experimental confirmation of this theoretical approach as an effective low-energy theory of interacting bosons in one dimension and demonstrates the power of quantum noise analysis in studying strongly correlated many-body systems.

We expect our experiments to pave the way for other methods of characterizing many-body systems using the analysis of quantum noise such as particle number fluctuations[42] and spin noise[43–45]. From the point of view of analysing systems with strong interactions and correlations, this should enable cold-atom experiments to provide a complementary and different perspective to that provided by electron systems.

METHODS

PREPARING TWO INDEPENDENT 1D CONDENSATES ON AN ATOM CHIP

We start the experiment with a thermal ensemble of $\sim 10^5$ ^{87}Rb atoms in the $|F = 2, m_F = 2\rangle$ state at a temperature $T \approx 5\,\mu$K in a single highly elongated magnetic trap on an atom chip[27,28]. This initial sample is prepared using our standard procedure of laser cooling, magnetic trapping, and evaporative cooling[46]. The initial trapping configuration is then deformed in the transverse direction into a highly anisotropic double-well potential by means of radio-frequency- (rf-)induced adiabatic potentials[24,26]. In particular, we use the rf-trap set-up presented in ref. 25, where the combination of two rf fields generated by wires on the atom chip enables the realization of a compensated symmetric double-well potential in the vertical plane. The final cooling of the two separate ensembles leading to the two 1D condensates is achieved by carrying out forced evaporative cooling in the dressed state potential[47]. We observe the onset of quantum degeneracy at $T \approx 400\,$nK in each of the two potential tubes.

The potential barrier between the two systems is controlled by the amplitude of the rf fields and the gradient of the static magnetic trap[26]. We realize a barrier height $V \approx k_B \times 4\,\mu$K to ensure a complete decoupling of the two systems during the final cooling stage.

After cooling and a relaxation time of 300 ms to ensure each system is in equilibrium (a constant rf knife is kept on during this time to prevent heating), each potential tube contains 3,000–5,000 atoms at typical temperatures $T < 100\,$nK. The atoms are trapped in a strong transverse harmonic confinement of $\nu_\perp \sim 3.0\,$kHz (longitudinal confinement $\nu_\parallel = 5\,$Hz) at a distance of 75 μm from the atom chip surface. Each individual degenerate atomic ensemble is in the 1D regime, with both temperature T and chemical potential μ fulfilling $k_B T, \mu < h\nu_\perp$ (refs 29,30).

EXTRACTING THE FRINGE AMPLITUDE FROM INTERFERENCE PATTERNS

We observe the interference pattern created by the two expanding, overlapping atomic clouds using standard absorption imaging. For the vertical double-well orientation used in the experiments, the observed interference fringes in the atomic density are horizontal, parallel to the atom chip surface. This enables us to image the interference pattern along the transverse direction of the system. The used imaging system has a spatial resolution of 3.4 μm and a noise floor of $\sim$3 atoms per $3 \times 3\,\mu$m pixel. From a single interference image we obtain line profiles for different L by integrating the two-dimensional absorption

image over various lengths along the longitudinal direction of the system. The obtained line densities are then Fourier transformed, and we extract A_Q as the value of this Fourier transform at the wavevector Q corresponding to the observed fringe spacing. This spacing is determined from fitting the interference patterns with a cosine function with a gaussian envelope plus an unmodulated gaussian to account for the contrast reduction. The free parameters of these fits are the relative phase θ, the contrast, and the fringe spacing. The width, amplitude, and centre position of the total cloud are determined independently from a gaussian fit to the full integrated density pattern of the central area of each image. Note that the absolute value of the interference amplitude $|A_Q|$ (as defined in equation (1)) and the contrast C are related as $|A_Q| = n_{1D}\, L \times C$.

AVERAGE INTERFERENCE AMPLITUDE FITS

To compare the experimentally observed length dependence of the average interference amplitude to theory, we perform a least-square fit of the theoretical prediction equation (2) to the data. Because the line density n_{1D} is extracted directly from the absorption images and the transverse trapping frequency $\nu_\perp$ is measured precisely by parametric heating experiments, the only unknown experimental parameter is the temperature T. In addition to T as a fit parameter, we include a scaling factor ($\langle |A_Q|^2\rangle_{\mathrm{measured}} = S * \langle |A_Q|^2\rangle_{\mathrm{real}}$) to account for reduced contrast in the experimental data due to technical aspects. For all data sets we find $S \approx 0.4$, which is consistent with the maximum observed interference contrast of 65%. This contrast reduction is in agreement with an analysis of our imaging system, taking into account its limited resolution and focal depth, as well as a tilt of the imaging axis with respect to the double well.

LUTTINGER LIQUID

A 1D gas of ultracold bosonic atoms can be described by the Lieb–Liniger model of bosons interacting via a pointlike repulsion[22,48,49]. The effective approach to the Lieb–Liniger model, capturing the long-distance behaviour of all correlation functions, is known as the Luttinger liquid formalism[36–38]. The essence of this approach is to represent the original bosonic field in terms of the two phase fields $a(z) = (n_{1D} + \partial\theta(z))^{1/2} e^{i\phi(z)}$ and keep only the terms quadratic in $\phi(z), \theta(z)$ in the hamiltonian. The resulting theory has a linear spectrum of bosonic sound waves and shows algebraic decay of all correlation functions at zero temperature (for example $\langle a^\dagger a\rangle \sim |z_1 - z_2|^{1/2K}$) and exponential decay for finite temperature (for example $\langle a^\dagger(z_1) a(z_2)\rangle \sim n_{1D}[\pi/(\xi_T n_{1D} \sinh(\pi(z_1 - z_2)/\xi_T))]^{1/2K}$).

Here K is the fundamental parameter of the theory, the so-called Luttinger parameter, and $\xi_T = \xi_\phi(T)/K$. The last expression applies down to the short-distance cut-off given by the healing length. The value of K is uniquely determined by the dimensionless ratio characterizing the original microscopic model: $\gamma = mg/\hbar^2 n_{1D}$, where g is the 1D interaction strength. In the weakly interacting regime studied here, $K \approx \pi/\sqrt{\gamma}$. Recent analysis showed[50] that the Luttinger liquid formalism provides an extremely accurate description of the correlation functions of the Lieb–Liniger model for both long distances and distances just beyond the healing length.

CALCULATION OF THE DISTRIBUTION FUNCTIONS

Computation of the distribution functions requires, in principle, the knowledge of all moments of the interference fringe amplitude. One approach to overcome this problem of moments was introduced in ref. 18, where methods of conformal field theory and special properties of exactly solvable models were used to compute the distribution function for periodic boundary conditions at zero temperature. Another method, which enables us to compute the distribution functions for all boundary conditions, arbitrary temperature, and in all dimensions[41], is based on the mapping of the problem to a generalized Coulomb gas model and a related problem of fluctuating random surfaces (for a review, see ref. 31). This is the approach which we use in our analysis.

The full distribution function $W(\alpha)$ is defined by the normalized moments of the interference fringe contrast as

$$\langle \alpha^m \rangle = \langle |A_Q|^{2m}\rangle / \langle |A_Q|^2\rangle^m = \int_0^\infty W(\alpha)\alpha^m \,\mathrm{d}\alpha.$$

Using Luttinger liquid theory, these moments can be expressed[17] as the micro-canonical partition functions of the Coulomb gas of $2m$ particles

$$\langle \alpha^m \rangle = \alpha_0^{-m} \int_0^1 \ldots \int_0^1 \mathrm{d}u_1 \ldots \mathrm{d}v_m \times \exp\left[\frac{1}{K}\sum_{i<j}\{G(u_i,u_j) + G(v_i,v_j)\} - \frac{1}{K}\sum_{i,j} G(u_i,v_j)\right],$$

where

$$\alpha_0 = \int_0^1 \int_0^1 \mathrm{d}u_1\, \mathrm{d}v_1 \exp\left[-\frac{G(u_1,v_1)}{K}\right].$$

Here $G(x,y)$ is the interaction potential, whose precise form depends on the geometry of the problem and the temperature. At zero temperature $G(x,y) = \log|x-y|$, whereas at non-zero temperature $G_T(x,y) = \log((\xi_T/\pi L)\sinh(\pi|x-y|L/\xi_T))$. Real and symmetric $G(x,y)$ can be decomposed as $G(x,y) = \sum_{n=1}^{n=\infty} G_n \Psi_n(x)\Psi_n(y)$. Such decomposition is similar to diagonalization of a symmetric matrix by finding its eigenvectors and eigenvalues. Eigenfunctions $\Psi_n(x)$ and eigenvalues G_n of the interaction potential $G(x,y)$ can be used to construct the height variable $h(x,\{t_n\}) = \sum_n t_n T_n(x) - T_n(x)^2/2$, where $T_n(x) = \Psi_n(x)\sqrt{G_n/K}$ and t_n are fluctuating noise variables. Introducing $g(\{t_n\}) = \int \mathrm{d}x \exp[h(x,\{t_n\})]$, the distribution function can be written as[31,41]

$$W(\alpha) = \prod_{n=1}^{\infty} \frac{\int_{-\infty}^{\infty} \mathrm{d}t_n e^{-t_n^2/2}}{\sqrt{2\pi}} \delta[\alpha - \alpha_0^{-1} g(\{t_n\}) g(\{-t_n\})]. \quad (4)$$

We compute this function using a Monte Carlo algorithm. Random variables $\{t_n\}$ are chosen from the gaussian ensemble, and 1D integrals $g(\{t_n\}), g(\{-t_n\})$ are evaluated for each realization of $\{t_n\}$. According to equation (4), the distribution function $W(\alpha)$ coincides with the distribution function of the product $\alpha_0^{-1} g(\{t_n\}) g(\{-t_n\})$. In the limit of large parameters F equation (4) can be evaluated explicitly to show that the distribution approaches one of the extreme-value statistics distributions (similar to a Gumbel form)[31,40].

Received 28 November 2007; accepted 13 March 2008; published 20 April 2008.

References

1. Wheeler, J. & Zurek, W. *Quantum Theory and Measurement* (Princeton Univ. Press, Princeton, 1984).
2. Gardiner, C. W. & Zoller, P. *Quantum Noise* (Springer, Berlin, 2004).
3. Levitov, L. S. in *Quantum Noise in Mesoscopic Systems* (ed. Nazarov, Yu. V.) (Kluwer, Dordrecht, 2007).
4. Sukhorukov, E. V. *et al.* Conditional statistics of electron transport in interacting nanoscale conductors. *Nature Phys.* **3**, 243–247 (2007).
5. Samuelsson, P., Sukhorukov, E. V. & Büttiker, M. Two-particle Aharonov–Bohm effect and entanglement in the electronic Hanbury Brown–Twiss setup. *Phys. Rev. Lett.* **92**, 026805 (2004).
6. Neder, I. *et al.* Interference between two indistinguishable electrons from independent sources. *Nature* **448**, 333–337 (2007).
7. Altman, E., Demler, E. & Lukin, M. D. Probing many-body states of ultra-cold atoms via noise correlations. *Phys. Rev. A* **70**, 013603 (2004).
8. Fölling, S. *et al.* Spatial quantum noise interferometry in expanding ultracold atom clouds. *Nature* **434**, 481–484 (2005).
9. Rom, T. *et al.* Free fermion antibunching in a degenerate atomic Fermi gas released from an optical lattice. *Nature* **444**, 733–736 (2006).
10. Greiner, M., Regal, C. A., Stewart, J. T. & Jin, D. S. Probing pair-correlated fermionic atoms through correlations in atom shot noise. *Phys. Rev. Lett.* **94**, 110401 (2005).
11. Öttl, A., Ritter, S., Köhl, M. & Esslinger, T. Correlations and counting statistics of an atom laser. *Phys. Rev. Lett.* **95**, 090404 (2005).
12. Schellekens, M. *et al.* Hanbury Brown Twiss effect for ultracold quantum gases. *Science* **310**, 638–651 (2005).
13. Jeltes, T. *et al.* Comparison of the Hanbury Brown–Twiss effect for bosons and fermions. *Nature* **445**, 402–405 (2007).
14. Donner, T. *et al.* Critical behavior of a trapped interacting Bose gas. *Science* **315**, 1556–1558 (2007).
15. Richard, S. *et al.* Momentum spectroscopy of 1d phase fluctuations in Bose–Einstein condensates. *Phys. Rev. Lett.* **91**, 010405 (2003).
16. Hadzibabic, Z., Krüger, P., Cheneau, M., Battelier, B. & Dalibard, J. Berezinskii–Kosterlitz–Thouless crossover in a trapped atomic gas. *Nature* **441**, 1118–1121 (2006).
17. Polkovnikov, A., Altman, E. & Demler, E. Interference between independent fluctuating condensates. *Proc. Natl Acad. Sci. USA* **103**, 6125–6129 (2006).
18. Gritsev, V., Altman, E., Demler, E. & Polkovnikov, A. Full quantum distribution of contrast in interference experiments between interacting one dimensional Bose liquids. *Nature Phys.* **2**, 705–709 (2006).
19. Dettmer, S. *et al.* Observation of phase fluctuations in elongated Bose–Einstein condensates. *Phys. Rev. Lett.* **87**, 160406 (2001).
20. Esteve, J. *et al.* Observations of density fluctuations in a very elongated Bose gas: From the ideal gas to the quasi-condensate regime. *Phys. Rev. Lett.* **96**, 130403 (2006).
21. Tolra, B. L. *et al.* Observation of reduced three-body recombination in a correlated 1d degenerate Bose gas. *Phys. Rev. Lett.* **92**, 190401 (2004).
22. Kinoshita, T., Wenger, T. & Weiss, D. S. Observation of a one-dimensional Tonks–Girardeau gas. *Science* **305**, 1125–1128 (2004).
23. Paredes, B. *et al.* Tonks–Girardeau gas of ultracold atoms in an optical lattice. *Nature* **429**, 277–281 (2004).
24. Schumm, T. *et al.* Matter wave interferometry in a double well on an atom chip. *Nature Phys.* **1**, 57–62 (2005).
25. Hofferberth, S., Lesanovsky, I., Fischer, B., Verdu, J. & Schmiedmayer, J. Radio-frequency dressed state potentials for neutral atoms. *Nature Phys.* **2**, 710–716 (2006).
26. Lesanovsky, I. *et al.* Adiabatic radio frequency potentials for the coherent manipulation of matter waves. *Phys. Rev. A* **73**, 033619 (2006).
27. Folman, R., Krüger, P., Schmiedmayer, J., Denschlag, J. & Henkel, C. Microscopic atom optics: From wires to an atom chip. *Adv. At. Mol. Opt. Phys.* **48**, 263–356 (2002).
28. Fortagh, J. & Zimmermann, C. Magnetic microtraps for ultracold atoms. *Rev. Mod. Phys.* **79**, 235–290 (2007).
29. Petrov, D. S., Gangardt, D. M. & Shlyapnikov, G. V. Low-dimensional trapped gases. *J. Phys. IV* **116**, 5–44 (2004).

30. Bouchoule, I., Kheruntsyan, K. V. & Shlyapnikov, G. V. Interaction-induced crossover versus finite-size condensation in a weakly interacting trapped one-dimensional Bose gas. *Phys. Rev. A* **75**, 031606(R) (2007).
31. Imambekov, A., Gritsev, V. & Demler, E. in *Proc. 2006 Enrico Fermi Summer School on Ultracold Fermi Gases* (eds Inguscio, M., Ketterle, W. & Salomon, C.) (IOS Press, Amsterdam, 2007).
32. Castin, Y. & Dalibard, J. Relative phase of two Bose–Einstein condensates. *Phys. Rev. A* **55**, 4330–4337 (1997).
33. Javanainen, J. & Wilkens, M. Phase and phase diffusion of a split Bose–Einstein condensate. *Phys. Rev. Lett.* **78**, 4675–4678 (1997).
34. Leggett, A. J. Bose–Einstein condensation in the alkali gases. *Rev. Mod. Phys.* **73**, 307–356 (2001).
35. Popov, V. N. *Functional Integrals in Quantum Field Theory and Statistical Physics* (Reidel, Dordrecht, 1983).
36. Haldane, F. Effective harmonic-fluid approach to low-energy properties of one-dimensional quantum fluids. *Phys. Rev. Lett.* **47**, 1840–1843 (1981).
37. Giamarchi, T. *Quantum Physics in One Dimension* (Oxford Univ. Press, Oxford, 2003).
38. Cazalilla, M. Bosonizing one-dimensional cold atomic gases. *J. Phys. B* **37**, S1–S47 (2004).
39. Polkovnikov, A. Shot noise of interference between independent atomic systems. *Europhys. Lett.* **78**, 10006–10010 (2007).
40. Gumbel, E. J. *Statistics of Extremes* (Columbia Univ. Press, New York, 1958).
41. Imambekov, A., Gritsev, V. & Demler, E. Mapping of Coulomb gases and sine–Gordon models to statistics of random surfaces. Preprint at <http://cond-mat/0612011> (2006).
42. Belzig, W., Schroll, C. & Bruder, C. Density correlations in ultracold atomic Fermi gases. *Phys. Rev. A* **75**, 063611 (2007).
43. Eckert, K. *et al.* Quantum non-demolition detection of strongly correlated systems. *Nature Phys.* **4**, 50–54 (2008).
44. Cherng, R. & Demler, E. Quantum noise analysis of spin systems realized with cold atoms. *New J. Phys.* **9**, 7 (2007).
45. Eckert, K., Zawitkowski, L., Sanpera, A., Lewenstein, M. & Polzik, E. S. Quantum polarization spectroscopy of ultracold spinor gases. *Phys. Rev. Lett.* **98**, 100404 (2007).
46. Wildermuth, S. *et al.* Optimized magneto-optical trap for experiments with ultracold atoms near surfaces. *Phys. Rev. A* **69**, 030901 (2004).
47. Hofferberth, S., Fischer, B., Schumm, T., Schmiedmayer, J. & Lesanovsky, I. Ultracold atoms in radio-frequency dressed potentials beyond the rotating-wave approximation. *Phys. Rev. A* **76**, 013401 (2007).
48. Olshanii, M. Atomic scattering in presence of an external confinement and a gas of impenetrable bosons. *Phys. Rev. Lett.* **81**, 938–941 (1998).
49. Lieb, E. & Liniger, W. Exact analysis of an interacting Bose gas. i. The general solution and the ground state. *Phys. Rev.* **130**, 1605–1616 (1963).
50. Caux, J.-S., Calabrese, P. & Slavnov, N. A. One-particle dynamical correlations in the one-dimensional Bose gas. *J. Stat. Mech.* **0701**, P008 (2007).

Acknowledgements

We acknowledge financial support from the European Union through the contracts MRTN-CT-2003-505032 (Atom chips), Integrated Project FET/QIPC 'SCALA', FWF, NSF, Harvard-MIT CUA, AFOSR, Swiss NSF and MURI. We thank S. Groth for fabricating the atom chip used in the experiments and D. A. Smith for critical reading of the manuscript.

Author contributions

S.H. and J.S. collected the data presented in this article. A.I., V.G., and E.D. provided the theoretical models used. All authors contributed to analysis and interpretation of the data and helped in editing the manuscript.

Author information

Reprints and permission information is available online at http://npg.nature.com/reprintsandpermissions. Correspondence and requests for materials should be addressed to J.S.